Electron diffraction of foam-like clusters between xenon and helium in superfluid helium droplets

Marisol Trejo, Andrew Clifford, Ernesto García-Alfonso, Nadine Halberstadt, Lan Xue, Wei Kong

Electron diffraction of foam-like clusters between xenon and helium in superfluid helium droplets

Marisol Trejo,[1] Andrew Clifford,[1] Ernesto Garcia Alfonso,[2] Nadine Halberstadt,[2] Lan Xue,[3] and Wei Kong[1*]

1. Department of Chemistry, Oregon State University, Corvallis, Oregon, 97331, USA
2. Labo Collisions, Agrégats, Réactivité (LCAR) Université de Toulouse and CNRS, 118 route de Narbonne, 31062 Toulouse CEDEX 09, France
3. Department of Statistics, Oregon State University, Corvallis, Oregon, 97331, USA

Manuscript for submission to J. Chem. Phys., 7/14/2024

*corresponding author, Wei.Kong@oregonstate.edu, 1-541-737-6714.

Abstract

We report electron diffraction results of xenon clusters formed in superfluid helium droplets, with droplet sizes in the range of 10^5 – 10^6 atoms/droplet, and xenon clusters from a few to a few hundred atoms. Under four different experimental conditions, the diffraction profiles can be fitted using four atom pairs of Xe. For the two experiments performed with higher helium contributions, the fittings with one pair of Xe-He and three pairs of Xe-Xe distances are statistically preferred compared with four pairs of Xe-Xe distances, while the other two experiments exhibit the opposite preference. In addition to the shortest pair distances corresponding to the van der Waals distances of Xe-He and Xe-Xe, the longer distances are in the range of the different arrangements of Xe-He-Xe and Xe-He-He-Xe. The number of independent atom pairs are too many for the small xenon clusters and too few for the large clusters. We consider these results evidence of xenon foam structures, with helium atoms stuck between Xe atoms. This possibility is confirmed by helium time-dependent density functional calculations. When the impact parameter of the second xenon atom is a few Angstroms or longer, the second xenon atom fails to penetrate the solvation shell of the first atom, resulting in a dimer with a few He atoms in between the two Xe atoms. In addition, our results for larger droplets point towards a multi-center growth process of dopant atoms or molecules, which is in agreement with previous proposals from theoretical calculations and experimental results.

1. Introduction

One of the major motivations in studies of clusters is to understand the structure and property transitions from single atoms or molecules to the bulk.[1] On this front, rare gas clusters are known to exhibit a crystal structure problem,[2] i.e. small clusters of rare gas atoms other than helium tend to form structures with five-fold symmetry axes, such as pentagonal bipyramidal or icosahedral, which are incompatible with the face-centered cubic (FCC) structure of the three-dimensional (3D) crystal lattices.[3] The polyicosahedral (PIC) structures contain multiple twined icosahedrons, or with increasing size, multiple layers of strained icosahedrons. They were initially deduced from the simple packing arrangement and were later confirmed from theoretical optimizations using Lennard-Jones potentials.[4-8] Electron diffraction (ED) studies of clusters containing tens to thousands of atoms also agree with the prevalence of the PIC structures for small clusters,[6,9-13] and searches for the size to transition from PIC to FCC have led to the speculation that both structures coexist and the dominant structure switches from PIC to FCC at cluster sizes containing a few hundred to a few thousand atoms.[7,8,11,12,14]

The clusters from previous experimental studies are formed from supersonic jets and the cluster sizes are determined using the scaling law.[7,8,11,12,14] With the invention of superfluid helium droplets, clusters of different sizes can be easily formed using the pickup method, and the resulting cluster sizes follow the Poisson distribution.[15-22] Hence clusters small and large can be controlled by the doping condition, including the pressure and doping distance. This capability affords a fresh new investigation of the structures of rare gas clusters.[23]

The environment inside superfluid helium droplets is different from vacuum, and the formation mechanism of clusters may differ from that of supersonic expansion, or from that of typical crystal growth. The resulting cluster structure may also be unique and different from that of the gas phase or the bulk. In one of our previous investigations, we discovered that iodine molecular clusters form halogen bonds inside superfluid helium droplets, with an intermolecular distance much shorter than the van der Waals distances between two iodine atoms.[24] Other examples of unique structures of molecular clusters have also been reported, including the linear chain structure of HCN,[25] the foam-like structure of Mg with helium,[26-28] filament-like clusters of Xe and Ag,[29,30] and a group of clusters within the same droplet due to multi-center growth.[31] A contributing factor to this abnormal behavior is the ultracold temperature of the droplets, as well as fast energy dissipation in superfluid helium: at 0.4 K,

incoming monomers fail to localize at the global minimum before being [31]stuck in the metastable positions. In addition, the presence of vortices inside large droplets offers an additional controlling factor for dopant aggregation.[29,30]

The capturing and clustering processes of dopants in helium droplets have been studied theoretically using a variety of approaches, including helium time-dependent density functional theories (^{4}He-TDDFT).[32-38]An argon cluster formed inside a $^4He_{5000}$ is found to adopt a compact, gas-phase-like cluster, or a loosely bound metastable cluster with a substantial helium density caged inside.[36] The cluster growth is significantly hindered by the helium host due to the impeding shell structure around the dopants and due to kinematic effects that freeze the growing cluster in metastable configurations.[36,32]

In this report, we observe electron diffraction of xenon clusters formed in superfluid helium droplets under different droplet sizes and different xenon concentrations. Our diffraction profiles are quite different from those obtained from clusters formed from supersonic expansion, with no obvious PIC regardless of the size of the xenon clusters. Fitting of the experimental diffraction profiles results in four pair distances, with the shortest distances in general agreement with the van der Waals distances between two Xe atoms or between Xe and He. The contributions of the longer distances are generally too large, and the contribution of the atoms is too small, compared to any reasonable PIC structures. With the help of modeling, we assign the observed structures as dilute structures with helium in between xenon atoms, and/or in larger droplets as xenon foams in which several dilute xenon clusters grow independently of each other. This observation confirms the previous hypothesis that dense shells of He atoms around a dopant can impede aggregation and thus lead to independent "seeds" within a droplet, a seed being a dopant atom or cluster surrounded by several shells of tightly bound helium.[15] It also confirms the prediction from ^{4}He-TDDFT and atomistic simulations that the structures formed in droplets are not necessarily the same ones as in the gas phase.[36,38]

2. Experimental setup

The experimental setup includes the droplet source, the sample doping region, and the electron diffraction component, and details of the setup have been described in our previous publications.[23,39,40] In the source chamber, the helium stagnation pressure is kept at 70 atm, and the size of the droplets is controlled by the stagnation temperature, varying from 10 K to

18 K. In the doping chamber, gaseous xenon is released via a sample pulse valve (SPV), and depending on the size of the droplets, the doping pressure is adjusted by varying the duration of the SPV. In the diffraction chamber, a pulsed electron beam with an energy of 40 keV, duration of 30 μs, current of approximately 1 mA, beam diameter of 3 mm, and coherent length of approximately 300 nm is used to irradiate the doped helium droplets. The scattered electrons hit a phosphor screen and the image is captured by an Electron Multiplying Charge-Coupled Device. A Faraday cup centered at the phosphor screen collects the unscattered electrons to protect the screen and to measure the current of the electron beam.

The diffraction images are accumulated using active background subtraction. The SPV and the electron beam operate at 10 Hz, while the helium pulse valve operates at 5 Hz. The difference between the images obtained while the helium pulse valve is on vs. off removes the signal from the diffused xenon sample in the diffraction chamber. Additionally, the radial profile for neat helium droplets without the dopant gas is obtained using the same method, and the profile will be used in fitting the final diffraction results (see next section). The averaged diffraction images are processed into radial profiles, excluding the central patch of the Faraday cup and the wedge blocked by the support arm of the cup.

The size of the droplet is characterized before each diffraction experiment. Neat helium droplets are ionized by electron impact, and the time-of-flight (TOF) measurements of the ionized droplets are used to determine the mass of the droplets.[41] The approximate size of the xenon clusters embedded in the superfluid helium droplets is estimated using the Poisson distribution.[42] This estimation depends on the pickup cross-section of the droplet and the experimental doping pressure of the gaseous sample (number density of xenon).[42] All experiments are performed under the "overdoping" conditions,[43] with a significant fraction of the helium removed by the doping gas at relatively high pressures. This effect is somewhat similar to that of electron impact ionization where smaller droplets are destroyed, and larger droplets are reduced in size. Consequently, the measured helium droplet sizes from our TOF mass spectrometer are larger than those under similar stagnation conditions,[44,45] and these sizes are considered representative of the droplet sizes under our doping conditions. We note that the size distribution from our nozzle is bimodal with a velocity slip between the two groups of droplets,[46] and by timing the electron gun, we can also choose the larger size group.

3. Method of fitting

Gas phase electron diffraction without sample orientation consists of contributions from atoms and atom pairs, as shown in Eq. 1:

$$I(s) = \frac{K^2 I_0}{R^2}\sum_{n=1}^{N}[f_n(s)]^2 + \frac{K^2 I_0}{R^2}\sum_{n=1}^{N-1}\sum_{m=n+1}^{N}[f_n(s)]\,[f_m(s)]cos\,[\eta_n(s) - \eta_m(s)]\frac{sin\,(sr_{nm})}{sr_{nm}}, \quad (1)$$

where K is a constant, I_0 is the intensity of the incident electron beam, R is the distance between the scattering center and the detector, s is the momentum transfer between the incident and scattered wave, N is the total number of atoms in the sample, $f_n(s)$ is the scattering amplitude of the atom n at s, η_n is the phase shift of the scattered wave, and r_{nm} is the distance between atomic pairs, the only information carrier of the structure. The indices m and n represent atomic pairs without double counting. Some pair distances are the same by symmetry or by the nature of the chemical bonding, and in the following discussion, we call the number of identical pair distances "repeats". For each geometric structure of a cluster, there is a fixed ratio between the number of repeats of each unique pair distance. The simulated diffraction pattern also contains concentric rings, and a radial profile alone is sufficient to represent the experimental data.

When the sample is embedded inside superfluid helium droplets, the helium atoms also contribute to the observed intensity. During sample doping, some helium atoms are removed through evaporative cooling. This occurs due to the kinetic energy of the sample and the binding energy to the helium droplet and from cluster formation. To fit the observed experimental data, the contribution of helium is adjusted, as shown in Eq. 2:

$$I_{Fit} = A \times I_{He} + \left(B_1 \times I_{Pair_1} + B_2 \times I_{Pair_2} + \cdots + B_i \times I_{Pair_i}\right) + C \times I_{Xe} + D\,, \quad (2)$$

where I_{He} is the radial profile of the experimental diffraction pattern from neat droplets without sample doping, and A is the adjustable scaling factor, representing the fraction of remaining helium atoms after sample doping. In the above equation, the simulated profile of each atom pair is treated independently as I_{Pair_i}, and the contribution of each pair is

represented by the adjustable coefficient B_i. The contribution of xenon atoms is represented by I_{Xe} and the adjustable coefficient C, while D is the baseline correction of the radial profile largely due to leaked ambient light.

The absolute values of coefficients B_i and C are meaningless since the intensities are calculated from the scattering factors, while the observed intensity is dependent on the response of the phosphor screen and the gain of the camera. However, the ratios of these coefficients represent the relative abundance of each atom pair and the number of atoms. If any fixed structures are present, the ratios are of fixed values. For example, a dimer of xenon ($i = 1$) contains 2 atoms and 1 atomic pair, so the ratio of $C : B_1$ should be 2:1. As the size of the cluster increases, new pairs are formed, thereby increasing the molecular contribution of each unique pair distance. Table 1 lists the number of unique pair distances, the repeats of each distance, and the relative contributions of atoms, assuming the highest level of symmetry and the most compact 3D structure for each cluster size.

Table 1. List of atomic pairs and repeats for different clusters with compact 3D structures, from the shortest to the longest distances.

Cluster size (# of atoms)	Pair 1	Pair 2	Pair 3	Total Pairs	Structure
2	1			1	Linear
3	3			3	Equilateral Triangle
4	6			6	Tetrahedron
5	9 (3+6)*	1		10	Trigonal Bipyramid
6	12	3		15	Octahedron
7	15 (5+10)*	5	1	21	Pentagonal Bipyramid
8	12	12	4	28	Cube
13	42 (30+12)*	30	6	78	Icosahedron

** The number of edges on the base and the number of edges to the top and bottom apexes.*

A few observations can be made from Table 1. The total number of pairs increases as (*N(N-1))/2*) with *N* being the number of Xe atoms, consequently the ratio between the total number of pairs and the number of atoms increases linearly with a slope of 0.5. Between dimer and tetramer, there is only one unique pair distance which corresponds to the van der Waals distance. The only difference in the diffraction pattern of these 3 small clusters is the relative

contributions of atoms and atomic pairs: the ratio between the number of pairs and atoms increases as the size of the cluster grows, from 2:1 to 4:6. In general, atoms in larger clusters have higher effective coordination numbers, therefore the contribution of atoms gradually decreases relative to the number of total atomic pairs. Considering any structure in Table 1, pair distances longer than 'pair 1' (the shortest distance in each shape) are less abundant. This means that even in a cluster exhibiting high symmetry, shorter distances should dominate over longer distances. Clusters with less symmetry may contain more variation in longer pair distances.

Table 1 assumes that the most compact and the most symmetric structures should be formed for a xenon cluster since all atoms in the cluster are the same. However, we also need to consider possibilities of other structures, for example, a linear long chain of atoms as reported from ultrafast x-ray diffraction.[29,30,47] Doped atoms are attracted to vortices in large droplets, which can lead to the formation of long filament-shaped clusters. Diffraction patterns from the coherence of different vortex lines have been observed. Droplets as small as 5,000 atoms/droplet have been found theoretically to accommodate a vortex,[36] although experimental reports have been limited to sizes above 10^7 atoms/droplets.[47] A linear chain of xenon clusters should have a regular period of oscillation in the diffraction pattern since all pair distances are multiples of the nearest neighbor van der Waals distance. The ratios of the atomic to pair distances should also have a regular pattern: N(atom):(N-*1*):(N-*2*)…, in the order of increasing pair distances, i.e. a monotonic decay in the coefficients of the pair distances.

Another possibility, although physically unlikely, is planar structures, which result in larger pair distances than those listed in the 3D structures in Table 1. This possibility is excluded from the fitting results in the following discussion.

Without prior knowledge of the general structure of the sample, Eqs. 1 and 2 show that only pair distances can be determined from the diffraction profile of the randomly oriented sample. If the relative ratios of the contributions from the pair distances match the ratios listed in Table I, then a definitive structure of the sample can be determined.

The fitting program minimizes the sum of squared residuals using a nonlinear least-squares algorithm called 'lsqnonlin' from MATLAB. Coefficients and distances are constrained within this algorithm and reasonable initial values are assigned to both. To better find the

global minimum instead of local minima, the fitting program employs the 'MultiStart' function from MATLAB. This function runs the above minimization with various starting values to better sample the parameter space. Ten iterations were chosen because this resulted in the best reproducibility regardless of initial values.

We typically constrain the distances to be between 4 and 10 Å and choose a number of independent distances to fit the experimental data. To compare the relative quality of the different fitting results, we use two criteria. Firstly, the Akaike information criterion (AIC) is defined as

$$AIC = m * ln\left(\frac{SSR}{m}\right) + 2k\,, \tag{3}$$

where m is the number of data points (sample size), SSR is the Sum of Squared Residuals, and k is the number of fitting parameters.[48] Models are considered equivalent when their AIC difference is $\leqslant 2$,[49] while a model is strongly preferred when its AIC is lower by more than 10 than the AICs of other models.

Alternatively, the Bayesian information criterion (BIC) places a higher penalty on the number of fitting parameters:

$$BIC = m * ln\left(\frac{SSR}{m}\right) + k * ln\, m\,, \tag{4}$$

by scaling the number of parameters with the natural log of the number of data points.[50] The AIC is more lenient towards model complexity and often favors more complex models. In contrast, the BIC imposes a stronger penalty for complexity, thereby promoting simpler models. It is desired when the focus is on model parsimony and on avoiding overfitting.[50]

4. Results

4.1 Small droplet size at low doping pressure

We performed four diffraction experiments under different conditions: three different nozzle temperatures were used, resulting in three different droplet size distributions, and for the smallest droplet size produced at a nozzle temperature of 18 K, we used two different doping pressures. Figure 1 shows the radial profiles of the diffraction images accumulated at a droplet size of 3.9×10^5 atoms/droplet obtained at a nozzle temperature of 18 K and an

average doping pressure of 9.4×10^{-6} torr in the doping chamber. Based on Poisson statistics, there should be on average 1 - 3 xenon atoms per droplet. For reference, this condition is referred to as "18 K at low doping pressure" in the following discussion. The experimental data were collected from 110,876 images, corresponding to a total exposure time of 3.3 s.

The main panel of Fig. 1 is the diffraction profile only associated with the embedded xenon clusters, while the total diffraction profile, including helium, is shown in the inset. The residuals from the fitting are shown in the bottom panel, with magnitudes less than 1/10 of that of the main panel. At the current low doping pressure, a small fraction of the helium droplets are destroyed in the doping region before the droplet can reach the diffraction region, and for those droplets that can reach the diffraction region, a fraction of the helium atoms (560 He atoms per Xe out of 3.9×10^5 atoms/droplet[15]) from each droplet has evaporated due to cooling of the embedded xenon atoms. Nevertheless, the majority of the diffraction signal originates from the helium atoms due to their large number, hence the total diffraction profile shows almost no signs of atomic interference, as shown in the inset. The atomic coherence is only observable after the removal of the helium contribution. The residuals show no regular oscillations, implying that the fitting captures the essential oscillations generated by the coherent pairs.

The values of the BIC show a minimum when 4 atomic pairs are modeled, while the values of AIC continuously decrease with increasing number of pair distances. The change in the AIC value from 4 to 5 pairs, however, is less than 2, suggesting that 4 pair distances are adequate to model the diffraction profile. Table 2 shows the resulting values for the pair distances, the coefficient of each, and contributions of helium atoms, xenon atoms, and the baseline correction.

Table 2. Fitting results from diffraction profiles of small droplets (18 K, average size: 3.9×10^5 atoms/droplet) at low doping pressure (most probably Xe atoms/droplet: 2).

Pair Distance (Å)	Dist. Uncertainty	Coefficient (B_i)	Coeff. Uncertainty	Rel. Abound.*
4.39	0.01	3.30	0.10	0.40
6.96	0.08	1.91	0.34	0.23
7.70	0.15	1.73	0.37	0.21

8.60	0.13	1.27	0.30	0.15
Contribution		**Coefficient**	**Uncertainty**	
Helium (A)		6.78×10^{-1}	4×10^{-4}	
Xe Atom (C)		2.04	0.12	4.0[#]
Scalar (D)		6.21	0.53	

* *The ratio of the coefficients* (B_i) *to the sum of the coefficients* ($\sum B_i$).

[#] *The ratio of* $\sum B_i$ *to* C.

The fitting result is puzzling, although the agreement between experiment and fitting is remarkable. From Xe_2 to Xe_4, there should still be just one pair distance in the diffraction profile, and even for Xe_5, there should be only 2 or 3 (a less compact structure) pairs, and the longest pair should be much lower in contribution than that of the shortest pair. The shortest distance from the fitting is comparable to the van der Waals distance between two xenon atoms at 4.32 Å, but the ratio of the total coefficients for the atomic pairs to the coefficient of the atom ($\sum B_i : C$) is 4.0, exceeding the value expected for a small cluster with 1 - 3 atoms.

One major uncertainty in the experimental condition is the doping pressure, since doping was achieved from a pulse nozzle, and the relation between the measured pressure and the actual pressure has a large uncertainty. This error is particularly large when the doping pressure is only slightly higher than that of the base pressure (1.0×10^{-7} torr). A higher doping pressure than measured can result in a larger xenon cluster, resulting in the higher than usual contributions of pairs than atoms. Nevertheless, the condition for a most probable cluster size of 7 requires a doping pressure of approximately 3×10^{-5} torr, a value too far off the uncertainty based on our previous experience. On the other hand, even if the doping pressure is considerably underestimated, the ratios of the coefficients of the longest pair to the rest of the shorter pairs are still too high to be reasonable. According to Table 1, this ratio should be 1:20 (including 15 from pair 1 and 5 from pair 2), but in Table 2, this ratio is 0.15:0.84 ≈ 1:6.

To rationalize the need for four independent pair distances to fit the experimental data, we need to consider the possibility that perhaps helium atoms are playing a bigger role than just a mere outer shell solvent: the helium solvation shell of the first xenon atom may not be penetrated by the second xenon atom arriving into the same droplet. Consequently, one or

numerous helium atoms can be stuck in between two xenon atoms, resulting in longer Xe-Xe pair distances. The van der Waals radius of a helium atom is 1.4 Å,[51] but in liquid helium at 1 K, the average distance between helium atoms is 3.47 Å, corresponding to a radius of 1.74 Å.[52] A dimer of Xe-He has an equilibrium distance of 3.98 Å,[53] hence a linear Xe-He-Xe should have a Xe-Xe distance close to 8 Å. The second shortest distance from our fitting at 6.96 Å is shorter than 8 Å, while the longest distance at 8.6 Å is longer than that of the linear trimer. These distances may reflect the possibility that a single layer of loosely packed helium atoms surrounds each Xe or Xe_2.

The addition of helium atoms inside xenon clusters can qualitatively solve both the high number of independent pair distances and the relatively high ratio of coefficients of pair distances to that of xenon atoms. When one or two helium atoms are stuck in between the xenon atoms, the symmetry of the cluster breaks and all pair distances become independent. For example, a tetramer may require 6 independent pair distances to characterize. Helium has a much smaller diffraction amplitude compared with xenon ($f_{He}: f_{Xe} \approx 1:17$), and according to Eq. 1, the contribution of atomic scatterings from the helium atoms inside a cluster is negligible compared with that of xenon atoms. The contribution of Xe-He pairs, on the other hand, is more significant, therefore the presence of helium atoms inside a xenon cluster can increase the apparent contribution of atomic pairs in the fitting result. Unfortunately, including an additional Xe-He pair, in addition to the four Xe-Xe pairs, failed to improve the quality of the fitting based on the almost identical values of BIC. In this case, the simpler model without the Xe-He pair is statistically preferred. We suspect that this result may be an indication of the large amplitude of motion of the He atoms due to zero-point energy. For a dimer of Xe-He,[53] the full-width-at-half-max of the vibrational wavefunction is about 1.8 Å, about 40% of the pair distance between Xe-He (~4 Å). This large amplitude of motion will significantly dampen the oscillation in the diffracted wave, making it invisible to the experiment. T However, a slightly better fitting result, with reductions in AIC and BIC, was obtained by replacing one of the four Xe-Xe pairs with a Xe-He pair, and the results will be discussed in a later section.

A simulation of the Xe dimer formation inside a droplet of 1000 He atoms was conducted using helium time-dependent density functional theory. This theory, described extensively in Ref. [54] , has proven a powerful and reliable tool to describe the structure and dynamics of doped liquid helium and droplets. We used the BCN-TLS computing package[55] to simulate

the collision of one Xe atom with a He_{1000} droplet containing a Xe atom already stabilized in its center. The relative velocity between the droplet beam and the Xe projectile atom was set to be 170 m/s, and two values of the impact parameter b were tested: $b = 0$ ("head-on" collision) and $b = 11.1$ Å (half of the density radius of the droplet). The calculated collision processes are shown as movies in the supplementary material. In the head-on collision, the incoming Xe atom can penetrate the solvation shell and form a Xe_2, which rapidly relaxes to its equilibrium bond length as shown in Fig. 2. In the other case with $b = 11.1$ Å, the incoming Xe atom cannot penetrate through the He solvation shell, and the two Xe atoms rotate inside the droplet with a thick layer of He in between. These examples demonstrate that the clusters formed in droplets can be much less dense than those in the gas phase.

Possibilities of He sandwiched between dopant molecules and atoms have been reported from both experimental observations and theoretical calculations.[15,26-28,56-58] Increased helium density near the dopant, and lack of extra energy release due to cluster formation within the helium droplets, have both led to the picture of foam-like structured dopants. The dense shells of He atoms around a single dopant atom or molecule will impede the coagulation of other dopant atoms or molecules to produce larger aggregates. Further energy deposition into the foam-like structures embedded inside these droplets can collapse the loosely packed dopant structure, as evidenced from several studies.[26-28]

4.2 Small droplet size at high doping pressure

An additional experiment was performed with the small droplets by increasing the doping pressure to 2.8×10^{-5} torr, and the fitting results are listed in Table 3. The diffraction image was obtained from an average of 290,612 shots and a total exposure time of 8.7 s. Based on the droplet size, the most probable number of xenon atoms is expected to be 6 to 8.

Table 3. Fitting results from diffraction profiles of small droplets (18 K, average size: 3.9×10^5 atoms/droplet) at high doping pressure (most probable Xe atoms/droplet: 7).

Pair Distance (Å)	Dist. Uncertainty	Coefficient (B_i)	Coeff. Uncertainty	Rel. Abound.*
4.37	0.01	3.74	0.11	0.29
6.60	0.08	2.15	0.31	0.17
7.40	0.06	4.16	0.37	0.33

8.28	0.06	2.74	0.31	0.21
Contribution		**Coefficient**	**Uncertainty**	
Helium (A)		8.52×10^{-2}	5×10^{-4}	
Xe Atom (C)		1.68	0.12	$7.6^{\#}$
Scalar (D)		4.19	0.54	

* *The ratio of the coefficients* (B_i) *to the sum of the coefficients* ($\sum B_i$).

$^{\#}$ *The ratio of* $\sum B_i$ *to* C.

The change in the values of AIC and BIC is similar to the case of low doping pressure: the BIC shows a minimum with 4 pair distances, while the AIC shows a continuous decline but the change between 4 and 5 pairs is less than 4. We therefore chose to use 4 pair distances to model the diffraction profile. The contribution of helium is much lower – at 0.085 – under these conditions, compared with that under the lower doping pressure – 0.68. This means that the doping pressure is so high that only 8.5% of the helium atoms remain after doping, while 91.5% of the helium atoms are lost due to destruction by the xenon atoms or evaporative cooling.[59] The values of helium obtained from both fittings are in general agreement with the experimental observation: we use the diffraction intensity at s = 2.2 Å^{-1} as a reference, and the diffraction intensity drops by 90% when the doping pulse valve is on at high doping pressure.

The pair distances from Table 3 are also in general agreement with those of Table 2, but they are generally on the shorter side by about 0.3 Å except for the shortest distance corresponding to the van der Waals distance of Xe_2. The coefficient of atomic Xe is even smaller at the increased doping pressure, resulting in even higher contributions of atomic pairs. A higher doping pressure seems to have the effect of compacting the Xe cluster and increasing the coordination number of each atom.

Although the absolute values of the fitting coefficients $A - D$ in Eq. 2 are not meaningful, the trend in variation is still informative, particularly in this comparison between two different doping pressures when the droplet size remains the same. The contribution of Xe atoms (C) is slightly smaller than that for the low doping pressure conditions, which could be related to the massive loss of helium during doping, since the loss of small droplets also results in the

loss of doped xenon atoms embedded in these small droplets in the diffraction region. On the other hand, the increase in the ratio between the sum of the coefficients of the atomic pairs and the coefficient of the atom contribution (~7.6) at the higher doping pressure signifies increased coordination of each xenon atom due to the formation of larger structures. This result is in qualitative agreement with the doping statistics.

4.3 Larger droplet sizes and comparison of results

For the additional two experiments, we increased the droplet size by lowering the nozzle temperature to 12 K (5.2×10^5 He atoms/droplet) and 10 K (3.7×10^6 He atoms/droplet) and increased the doping pressure to 5.7×10^{-5} torr and 9.8×10^{-4} torr, resulting in a maximum xenon cluster containing 17-19 or approximately 947 atoms, respectively. The experimental data for these two conditions were collected from 165,652 images, corresponding to a total exposure time of 5.0 s, and 32,368 images, corresponding to a total exposure time of 0.97 s. Figure 3 shows the diffraction profiles obtained from all 4 doping conditions after removing the contributions of helium, and Tables 4 and 5 show the fitting results under these two conditions.

Figure 3 is extremely surprising, considering that with more than 900 xenon atoms in one droplet, there should be polyhedron structures of Xe, and the diffraction pattern should contain relatively sharper structures with more obvious modulations than those from small clusters, as observed in gas-phase electron diffraction experiments.[6,9-13,60] The experimental results from droplets show the opposite trend, with the smallest Xe clusters containing the most obvious modulation, while the largest cluster shows significantly attenuated modulation. It seems that the Xe clusters are somewhat amorphous, but they still contain some order.

Table 4. Fitting results from diffraction profiles of medium droplets (12 K, average size: 5.2×10^5 He atoms/droplet, most probable Xe atoms/droplet: 18).

Pair Distance (Å)	Dist. Uncertainty	Coefficient (B_i)	Coeff. Uncertainty	Rel. Abound.*
4.31	0.016	3.42	0.13	0.20
6.58	0.049	3.19	0.3	0.19
7.44	0.041	6.01	0.4	0.36

8.32	0.042	4.24	0.34	0.25
Contribution		**Coefficient**	**Uncertainty**	
Helium (A)		1.300×10^{-1}	5×10^{-4}	
Xe Atom (C)		2.75	0.15	6.1[#]
Scalar (D)		14.83	0.57	

* *The ratio of the coefficients* (B_i) *to the sum of the coefficients* ($\sum B_i$).

[#] *The ratio of* $\sum B_i$ *to* C.

Table 5. Fitting results from diffraction profiles of large droplets (10 K, average size: 3.7×10^6 He atoms/droplet, most probable Xe atoms/droplet: 947).

Pair Distance (Å)	**Dist. Uncertainty**	**Coefficient (B_i)**	**Coeff. Uncertainty**	**Rel. Abound.***
4.34	0.017	12.19	0.51	0.31
6.80	0.13	5.38	1.4	0.14
7.60	0.097	12.02	1.7	0.31
8.45	0.084	9.28	1.5	0.24
Contribution		**Coefficient**	**Uncertainty**	
Helium (A)		6.34×10^{-1}	3×10^{-3}	
Xe Atom (C)		18.18	0.76	2.1[#]
Scalar (D)		90.5	2.1	

* *The ratio of the coefficients* (B_i) *to the sum of the coefficients* ($\sum B_i$).

[#] *The ratio of* $\sum B_i$ *to* C.

The change in the values of AIC and BIC for the medium-size droplets at 12 K (5.2×10^5 He atoms/droplet) is similar to both cases of the small-size droplets, while at 10 K, the variation of the BIC also shows a minimum at 4 pair distances, but the AIC values drops by 7 with 5 pair distances, hence the simpler model with only 4 pair distances is chosen. We therefore

conclude that 4 pair distances are present in all four experimental conditions. This result is again surprising: with the much larger clusters, there should be many more pair distances, even for the most symmetric structure of icosahedron. Moreover, according to Table 1, the ratio of the number of pairs with the number of atoms increases with cluster size, and at the observed ratios of coefficients of pair distances to that of xenon atoms, 6:1 for 12 K and 2:1 for 10 K, the corresponding cluster sizes should be 13 and 5, far smaller than the estimated number of doped atoms. We therefore speculate that many small clusters are formed in these droplets, and these clusters distribute randomly inside the same droplet. This multi-center growth hypothesis agrees with the "multiple coagulation seeds" proposal by Lewerenz et al[15] in explaining the coagulation cross-section of a series of dopants, including rare gas atoms of Ar, Kr, and Xe atoms, and small molecules of SF_6 and H_2O.

The helium contribution at 12 K (0.13) is similar to that of 18 K at a high doping pressure (0.085), while the helium contribution at 10 K (0.63) is similar to that of 18 K at a low doping pressure (0.68). Interestingly, the resulting pair distances show a direct correlation with the helium content. Figure 4 compares the resulting 4 pair distances from the 4 doping conditions demonstrating the above correlations. The structures of Xe-He_2-Xe have two extremes, with He_2 either parallel or perpendicular to the axis of Xe-Xe. The range of these corresponding distances is marked on the horizontal axis.

From Fig. 4, the van der Waals distance is largely reproduced from all 4 doping conditions, and the larger distances show consistent patterns, with the two conditions containing lower helium contributions showing shorter distances, while the others consistently result in larger distances. This result alludes to the possibility that when most helium is removed in the doping region, there is a higher chance for a compact xenon cluster to form. Otherwise, helium atoms can be present in between xenon atoms, forming a "foam-like" structure. The two middle distances are both smaller than the Xe-Xe distance in a linear Xe-He-Xe trimer at 8 Å,[53] implying a relatively thin solvation shell of helium. It is therefore possible that with the adsorption of each successive Xe atom into the same helium droplet during doping, some adjustments of the solvation shell can occur, changing the distribution of pair-distances.

For all four experimental conditions, we tried to add a fifth pair distance corresponding to the Xe-He pair in the fitting, but failed to improve the fitting quality, with reductions in BIC values less than 2. However, for the two conditions with higher helium contributions, namely 18 K at low doping pressure and 10 K, replacing one of the four Xe-Xe pairs with a Xe-He

pair results in small but statistically significant improvements in the BIC, 3 for 18 K and 6 for 10 K source temperatures. A detailed study of one Xe-He pair distance with two to five Xe-Xe pairs found that the BIC was minimized at three Xe-Xe pairs for these data sets. The resulting coefficients and pair distances are shown in Fig. 5 where we compared the two fitting models, with model 1 containing the original four Xe-Xe pairs, and model 2 containing one Xe-He and three Xe-Xe pairs. In both models, the van der Waals distance is largely reproduced, and the shortest pair is the Xe-He pair, with values about 3.8 and 3.9 Å, slightly shorter than the Xe-He dimer distance from Sheng et al.[53] as shown by the star on the bottom axis. The contributions of the Xe-He pairs are the most significant, more than the sum of the rest of the three Xe-Xe pairs. From both statistical and physical considerations, model 2 is slightly more favored than model 1 under these two experimental conditions. This slight preference for the presence of the Xe-He pair further confirms the "foam-like" structure. However, for the other two experimental conditions with much less helium contributions in the fitting, replacing one of the four pairs of Xe-Xe results in significant increases in the values of AIC and BIC, by more than 20, therefore the fitting results presented in Tables 2 and 4 and Fig. 4 are still preferred.

The presence of the "foam-like" structure does not completely preclude the presence of neat Xe clusters with polyhedron structures. The experimental results are from an ensemble of droplets and clusters, and our results can only provide pair distances, not an exact structure of a cluster. In the gas phase, the presence of regular polyicosahedral clusters, relatively numerous even at the largest analyzed sizes, is attributed to kinetic effects in structure formation.[60] In superfluid helium droplets, perhaps it is a similar reason – kinetic effects in cluster formation – that prevents the formation of a neat polyicosahedron of xenon atoms, in the same way in which argon clusters were found to be frozen in metastable configurations in Ref. [38].

Nevertheless, the possibility of the "foam-like" structure is intriguing,[61] mainly because of the much stronger attractive binding energy between Xe atoms (~280 K) than that of Xe-He (~28 K).[53,62] Foam-like structures of neon in bulk superfluid helium have been predicted in theory,[32] and spectroscopic evidence from experiments has only reported on magnesium[26-28] and a few metal clusters.[63,64] Based on our calculation, the solvation energy of one Xe in a helium droplet of 1000 He atoms is ~289 K, on par with the binding energy of Xe-Xe. The solvation energy of Xe_2 should be larger than that of Xe, hence energetically, the formation

and solvation of Xe_2 is more favored than two independently solvated Xe atoms. The contribution of entropy at the temperature of the droplet of 0.4 K is limited. Using the lattice model explained in ref. [65], for a droplet containing 5×10^5 He atoms/droplet, assuming free translation and rotation of Xe and Xe_2 in the superfluid helium droplets, the entropy decrease is only on the order of 4 K upon dimerization, insufficient to make up the difference in solvation and internal energy. From a kinetics point of view, when angular momentum is present due to an impact parameter of the incident xenon atom, the total effective potential experienced by an incident xenon atom can become repulsive with a barrier of over 1 K, which can effectively prevent the penetration of the He solvation shell. According to Eloranta,[32] a dimer fails to be formed due to the energy cost of interpenetration of the solvent layers around each dopant atom. More results on different rare gas aggregates in superfluid helium droplets will certainly help with the understanding of the current speculation.

The pattern of the coefficients does not follow a monotonic decay, and the pair distances are not quite periodical, implying that even if some linear chains may exist due to vertices, linear structures of Xe atoms are not predominant. The shortest pair distance from the fitting matches the van der Waals distance between two xenon atoms, and no sign of covalent bonding exists in these clusters.[66,67]

Our results are in general agreement with those from ultrafast x-ray diffraction of Xe clusters in droplets.[29,30 47] The stagnation temperature of our pulsed nozzle is above ($\geq$ 10 K) the critical point of helium, and the droplet sizes are below 10^7 atoms/droplet. There should be very few if any vortices formed in the droplets. Although the report of Ulmer et al[47] also revealed the presence of Xe clusters inside large droplets, no detailed cluster structure was determined, largely due to the wavelength of the x-ray beam.

5. Conclusions

Using electron diffraction, we observed the formation of xenon clusters embedded in superfluid helium droplets. The diffraction patterns from four different experimental conditions can be simulated using four atomic pairs under all conditions. For the two experiments performed with higher helium contributions, the fittings with one pair of Xe-He and three pairs of Xe-Xe distances are statistically preferred compared with four pairs of Xe-Xe pairs, while the other two experiments exhibit the opposite preference. Although the quality of the fitting is remarkably high, the interpretation of the fitting results is difficult. In

particular, for the small clusters formed within small droplets under relatively low doping pressure, we are only expecting 1 or 2 independent atomic pairs, while for larger clusters, we would expect many more, far more than 4, atomic pairs. Moreover, the number of atomic pairs seems to be too large compared with the number of atoms in the fitting results. Our tentative explanation of these results is that helium atoms can be stuck in between two xenon atoms, and a "foam-like" structure of xenon and helium is formed. In addition, our results in larger droplets under high doping conditions could also point to multi-center growth of the xenon clusters. Further studies of other rare gas and metal clusters are ongoing in our laboratory to elucidate these possibilities.

Supplementary material

The supplementary document shows movies of the calculated processes of a second xenon atom colliding with a superfluid helium droplet with the first xenon atom at its center. Two scenarios with two different impact parameters are shown.

Acknowledgment

This material is based upon work supported by the National Institute of General Medical Sciences (GM149881) from the National Institutes of Health.

Data Availability Statement

The data that support the findings of this study are available from the corresponding author upon reasonable request.

References

1 B. Hartke, Angew. Chem., Int. Ed. **41**, 1468 (2002).

2 N. V. Krainyukova, Thin Solid Films **515**, 1658 (2006).

3 J. Farges, M. F. de Feraudy, B. Raoult, and G. Torchet, Adv. Chem. Phys. **70**, 45 (1988).

4 W. Wefelmeier, Z. Phys. **107**, 332 (1937).

5 M. R. Hoare and P. Pal, Advan. Phys. **20**, 161 (1971).

6 J. Farges, M. F. De Feraudy, B. Raoult, and G. Torchet, J. Chem. Phys. **78**, 5067 (1983).

7 J. W. Lee and G. D. Stein, J. Phys. Chem. **91**, 2450 (1987).

8 X. Shao, Y. Xiang, and W. Cai, J. Phys. Chem. A **109**, 5193 (2005).

[9] B. Raoult and J. Farges, Rev. Sci. Instrum. **44**, 430 (1973).

[10] J. Farges, M. F. De Feraudy, B. Raoult, and G. Torchet, J. Chem. Phys. **84**, 3491 (1986).

[11] O. G. Danylchenko, S. I. Kovalenko, and V. N. Samovarov, Low Temp. Phys. **30**, 166 (2004).

[12] O. G. Danylchenko, S. I. Kovalenko, and V. N. Samovarov, Low Temp. Phys. **30**, 743 (2004).

[13] O. G. Danylchenko, R. E. Boltnev, V. V. Khmelenko, V. Kiryukhin, O. P. Konotop, D. M. Lee, and N. V. Krainyukova, J. Low Temp. Phys. **187**, 156 (2017).

[14] J. Farges, M. F. De Feraudy, B. Raoult, and G. Torchet, Surf. Sci. **106**, 95 (1981).

[15] M. Lewerenz, B. Schilling, and J. P. Toennies, J. Chem. Phys. **102**, 8191 (1995).

[16] E. Loginov, L. F. Gomez, and A. F. Vilesov, J. Phys. Chem. A **115**, 7199 (2011).

[17] E. Latimer, D. Spence, C. Feng, A. Boatwright, A. M. Ellis, and S. F. Yang, Nano Lett. **14**, 2902 (2014).

[18] P. Thaler, A. Volk, D. Knez, F. Lackner, G. Haberfehlner, J. Steurer, M. Schnedlitz, and W. E. Ernst, J. Chem. Phys. **143**, 134201 (2015).

[19] L. Lundberg, P. Martini, M. Goulart, M. Gatchell, D. K. Bohme, and P. Scheier, J. Am. Soc. Mass Spectrom. **30**, 1906 (2019).

[20] M. Schnedlitz, R. Fernandez-Perea, D. Knez, M. Lasserus, A. Schiffmann, F. Hofer, A. W. Hauser, M. P. de Lara-Castells, and W. E. Ernst, J. Phys. Chem. C **123**, 20037 (2019).

[21] W. E. Ernst and A. W. Hauser, Phys. Chem. Chem. Phys. **23**, 7553 (2021).

[22] S. Albertini, E. Gruber, F. Zappa, S. Krasnokutski, F. Laimer, and P. Scheier, Mass Spectrom. Rev., 1 (2021).

[23] J. Zhang and W. Kong, Phys. Chem. Chem. Phys. **24**, 6349 (2022).

[24] Y. He, J. Zhang, L. Lei, and W. Kong, Angew. Chem., Int. Ed. **56**, 3541 (2017).

[25] K. Nauta and R. E. Miller, Science **283**, 1895 (1999).

[26] A. Przystawik, S. Goede, T. Döppner, J. Tiggesbäumker, and K.-H. Meiwes-Broer, Phys. Rev. A: At., Mol., Opt. Phys. **78**, 021202/1 (2008).

[27] S. Göde, R. Irsig, J. Tiggesbäumker, and K. H. Meiwes-Broer, New J. Phys. **15**, 015026 (2013).

[28] L. Kazak, S. Goede, K.-H. Meiwes-Broer, and J. Tiggesbaeumker, J. Phys. Chem. A **123**, 5951 (2019).

[29] L. F. Gomez, K. R. Ferguson, J. P. Cryan, C. Bacellar, R. M. P. Tanyag, C. Jones, S. Schorb, D. Anielski, A. Belkacem, C. Bernando, R. Boll, J. Bozek, S. Carron, G. Chen, T. Delmas, L. Englert, S. W. Epp, B. Erk, L. Foucar, R. Hartmann, A. Hexemer, M. Huth, J. Kwok, S. R. Leone, J. H. S. Ma, F. R. N. C. Maia, E. Malmerberg, S. Marchesini, D. M. Neumark, B. Poon, J. Prell, D. Rolles, B. Rudek, A. Rudenko, M. Seifrid, K. R. Siefermann, F. P. Sturm, M. Swiggers, J. Ullrich, F. Weise, P. Zwart, C. Bostedt, O. Gessner, and A. F. Vilesov, Science **345**, 906 (2014).

30 R. Fernandez-Perea, L. F. Gomez, C. Cabrillo, M. Pi, A. O. Mitrushchenkov, A. F. Vilesov, and M. P. de Lara-Castells, J. Phys. Chem. C **121**, 22248 (2017).

31 E. Loginov, L. F. Gomez, N. Chiang, A. Halder, N. Guggemos, V. V. Kresin, and A. F. Vilesov, Phys. Rev. Lett. **106**, 233401 (2011).

32 J. Eloranta, Phys. Rev. B: Condens. Matter Mater. Phys. **77**, 134301 (2008).

33 A. Hernando, M. Barranco, R. Mayol, M. Pi, and F. Ancilotto, Phys. Rev. B: Condens. Matter Mater. Phys. **78**, 184515/1 (2008).

34 J. Holler, E. Krotscheck, and R. E. Zillich, Eur. Phys. J. D **69**, 1 (2015).

35 F. Calvo, Phys. Rev. B **95**, 035429/1 (2017).

36 F. Coppens, F. Ancilotto, M. Barranco, N. Halberstadt, and M. Pi, Phys. Chem. Chem. Phys. **21**, 17423 (2019).

37 M. Blancafort-Jorquera, A. Vila, and M. Gonzalez, Phys. Chem. Chem. Phys. **21**, 24218 (2019).

38 E. Garcia-Alfonso, M. Barranco, D. A. Bonhommeau, N. Halberstadt, M. Pi, and F. Calvo, J. Chem. Phys. **157**, 014106 (2022).

39 J. Zhang, M. Trejo, S. Bradford, and W. Kong, J. Phys. Chem. Lett. **12**, 9644 (2021).

40 S. D. Bradford, M. Trejo, J. Zhang, W. Kong, and Y. Ge, J. Chem. Phys. **24** 27722 (2022).

41 J. Zhang, S. Bradford, and W. Kong, J. Chem. Phys. **152**, 224306 (2020).

42 M. Hartmann, R. E. Miller, J. P. Toennies, and A. F. Vilesov, Science **272**, 1631 (1996).

43 J. Zhang, Y. He, and W. Kong, J. Chem. Phys. **144**, 221101 (2016).

44 R. Sliter, L. F. Gomez, J. Kwok, and A. Vilesov, Chemical Physics Letters **600**, 29 (2014).

45 L. F. Gomez, E. Loginov, R. Sliter, and A. F. Vilesov, J. Chem. Phys. **135**, 154201 (2011).

46 R. Pandey, S. Tran, J. Zhang, Y. Yao, and W. Kong, J. Chem. Phys. **154**, 134303 (2021).

47 A. Ulmer, A. Heilrath, B. Senfftleben, S. M. O. O'Connell-Lopez, B. Kruse, L. Seiffert, K. Kolatzki, B. Langbehn, A. Hoffmann, T. M. Baumann, R. Boll, A. S. Chatterley, A. De Fanis, B. Erk, S. Erukala, A. J. Feinberg, T. Fennel, P. Grychtol, R. Hartmann, M. Ilchen, M. Izquierdo, B. Krebs, M. Kuster, T. Mazza, J. Montano, G. Noffz, D. E. Rivas, D. Schlosser, F. Seel, H. Stapelfeldt, L. Strueder, J. Tiggesbaeumker, H. Yousef, M. Zabel, P. Ziolkowski, M. Meyer, Y. Ovcharenko, A. F. Vilesov, T. Moeller, D. Rupp, and R. M. P. Tanyag, Phys. Rev. Lett. **131**, 076002 (2023).

48 H. Akaike, IEEE Trans. Autom. Control **19**, 716 (1974).

49 K. P. Burnham and D. R. Anderson, Sociol. Methods Res. **33**, 261 (2004).

50 G. Schwarz, Ann. Stat. **6**, 461 (1978).

51 A. Bondi, The Journal of Physical Chemistry **68**, 441 (1964).

[52] R. J. Donnelly and C. F. Barenghi, Journal of Physical and Chemical Reference Data **27**, 1217 (1998).

[53] X. Sheng, J. P. Toennies, and K. T. Tang, Physical Review Letters **125**, 253402 (2020).

[54] F. Ancilotto, M. Barranco, F. Coppens, J. Eloranta, N. Halberstadt, A. Hernando, D. Mateo, and M. Pi, Int. Rev. Phys. Chem. **36**, 621 (2017).

[55] M. Pi, F. Ancilotto, N. Halberstadt, A. Hernando, A. Leal, D. Mateo, R. Mayol, and M. Barranco, (https://github.com/bcntls2016/, 2016).

[56] R. N. Barnett and K. B. Whaley, Phys. Rev. A **47**, 4082 (1993).

[57] R. N. Barnett and K. B. Whaley, Z. Phys. D: At., Mol. Clusters **31**, 75 (1994).

[58] F. Dalfovo, Z. Phys. D: At., Mol. Clusters **29**, 61 (1994).

[59] Y. He, J. Zhang, and W. Kong, J. Chem. Phys. **144**, 084302 (2016).

[60] W. Polak, Phys. Rev. E: Stat., Nonlinear, Soft Matter Phys. **77**, 031404/1 (2008).

[61] A. Slenczka and J. P. Toennies, in Topics in Applied Physics, edited by A. Slenczka and J. P. Toennies (Springer, Switzerland, 2022), Vol. 145.

[62] R. Hellmann, B. Jäger, and E. Bich, J Chem Phys **147**, 034304 (2017).

[63] S. A. Krasnokutski and F. Huisken, J. Phys. Chem. A **115**, 7120 (2011).

[64] S. A. Krasnokutski and F. Huisken, J. Chem. Phys. **142**, 084311 (2015).

[65] K. A. Dill and S. Bromberg, Molecular Driving Forces. (Garland Science, London and New York, 2011).

[66] N. Bartlett, Proc. Chem. Soc., London, 218 (1962).

[67] D. A. Nelson and A. L. Ruoff, Phys. Rev. Lett. **42**, 383 (1979).

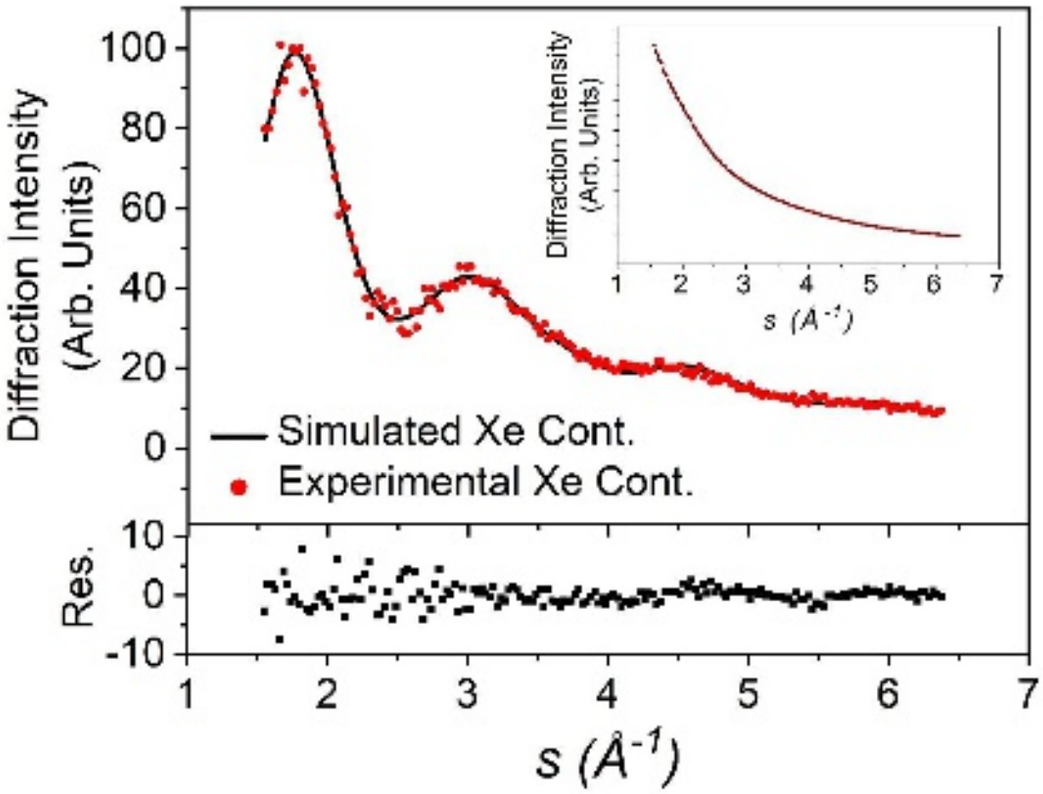

Fig 1. Radial profiles from electron diffraction of small droplets at low doping pressures. The inset shows the total diffraction profiles containing helium and the embedded xenon clusters, and the bottom panel shows the residuals in the same intensity unit as the main panel.

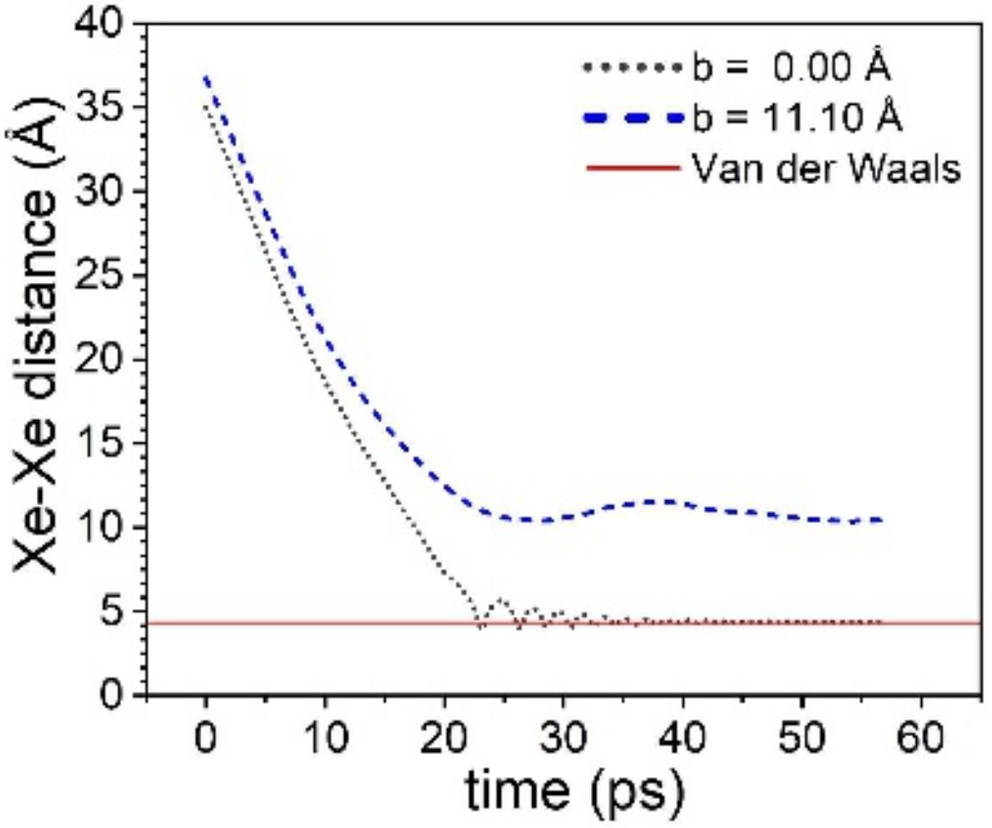

Fig. 2. Changes in distance between two xenon atoms at two different impact parameters. In the He-TDDFT calculation, one Xe atom is located at the center of a He droplet of 1,000 He atoms, and a second Xe atom approaches the droplet at two impact parameters as labeled. The van der Waals distance between two Xe atoms is labeled by the horizontal red line.

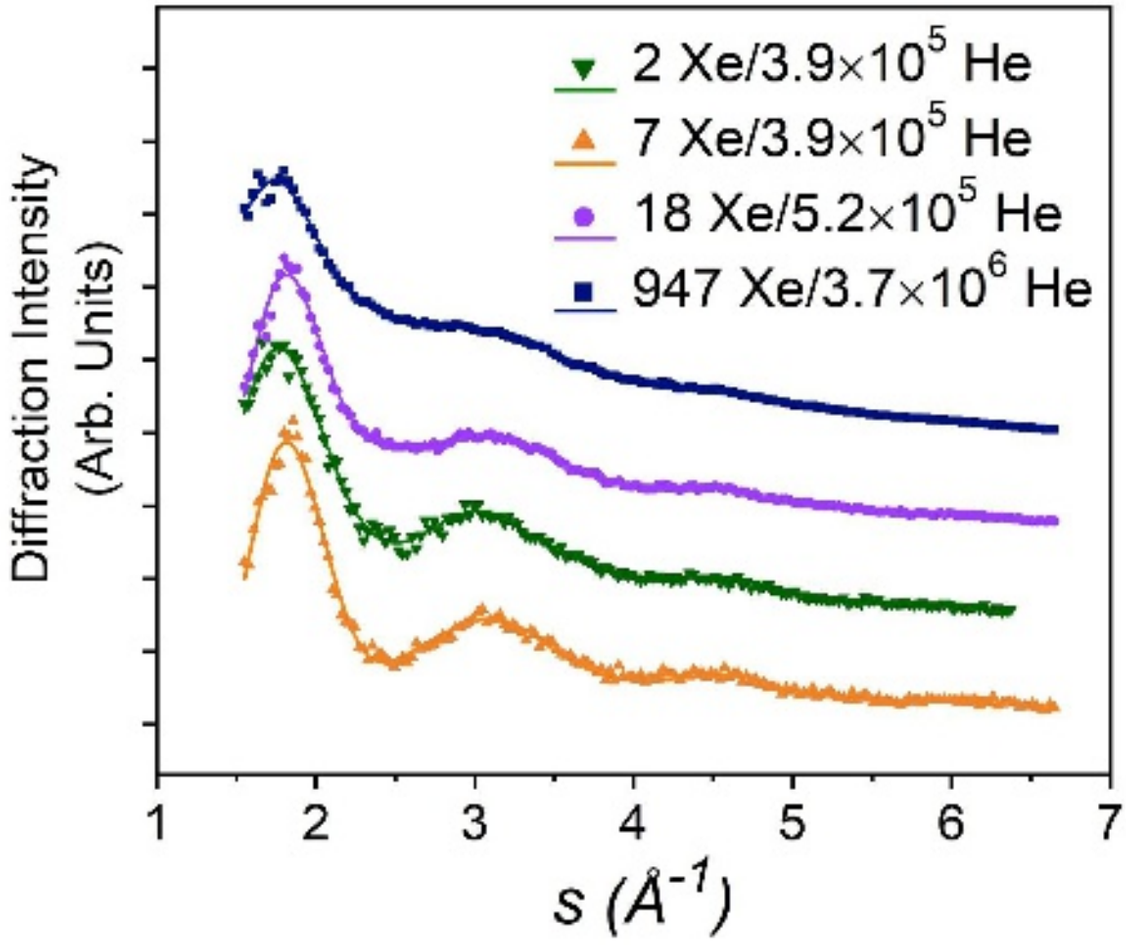

Fig. 3. Xenon contribution from all 4 conditions of diffraction. The two numbers in the legend label the most probable number of Xe and the average number of He atoms in a droplet. The symbols are derived from experimental results, and the continuous lines are the corresponding fitting results. The traces are shifted vertically for clarity.

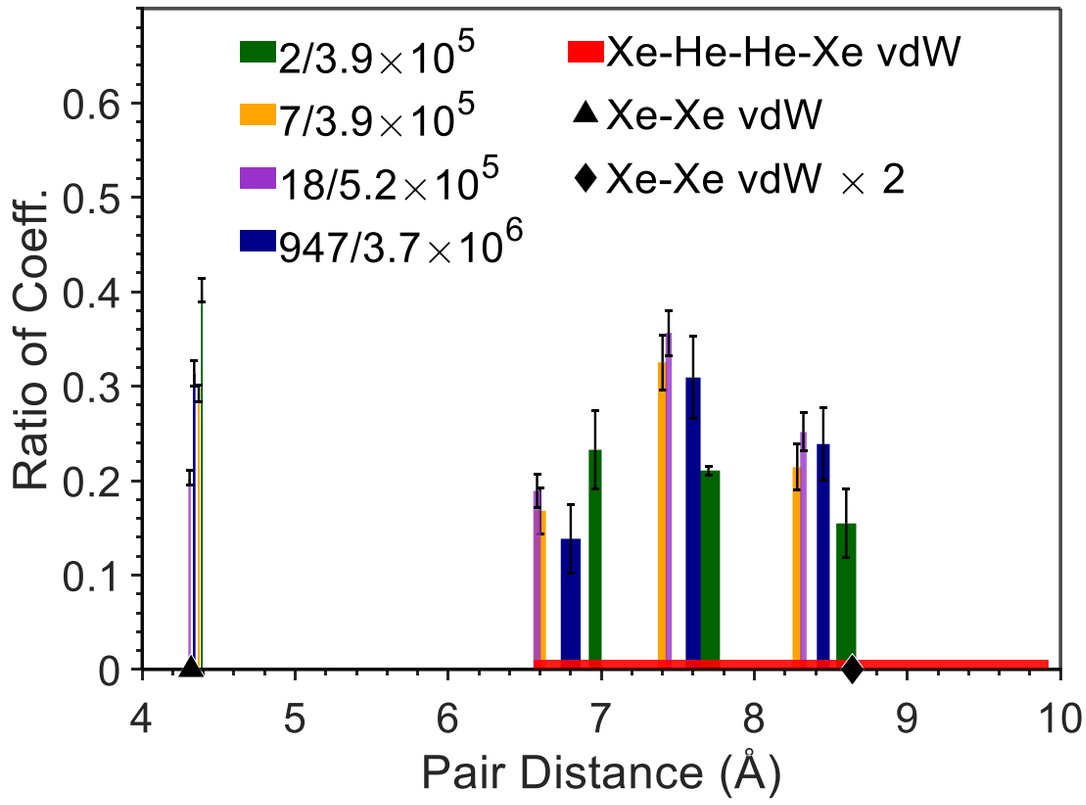

Fig. 4. Pair distances from fittings of all diffraction profiles. The widths of the bars represent the uncertainty of the distances, while the line segments on top of the bars represent the uncertainties in the coefficients. The two numbers in the legend label the numbers of Xe and He atoms in a droplet. The van der Waals distance between two xenon atoms is labeled by a triangle, twice of this distance corresponding to the end-to-end distance of a linear xenon trimer is labeled by a diamond, and the range of distances between all possible Xe-He-He-Xe structures is labeled by a red segment on the bottom axis.

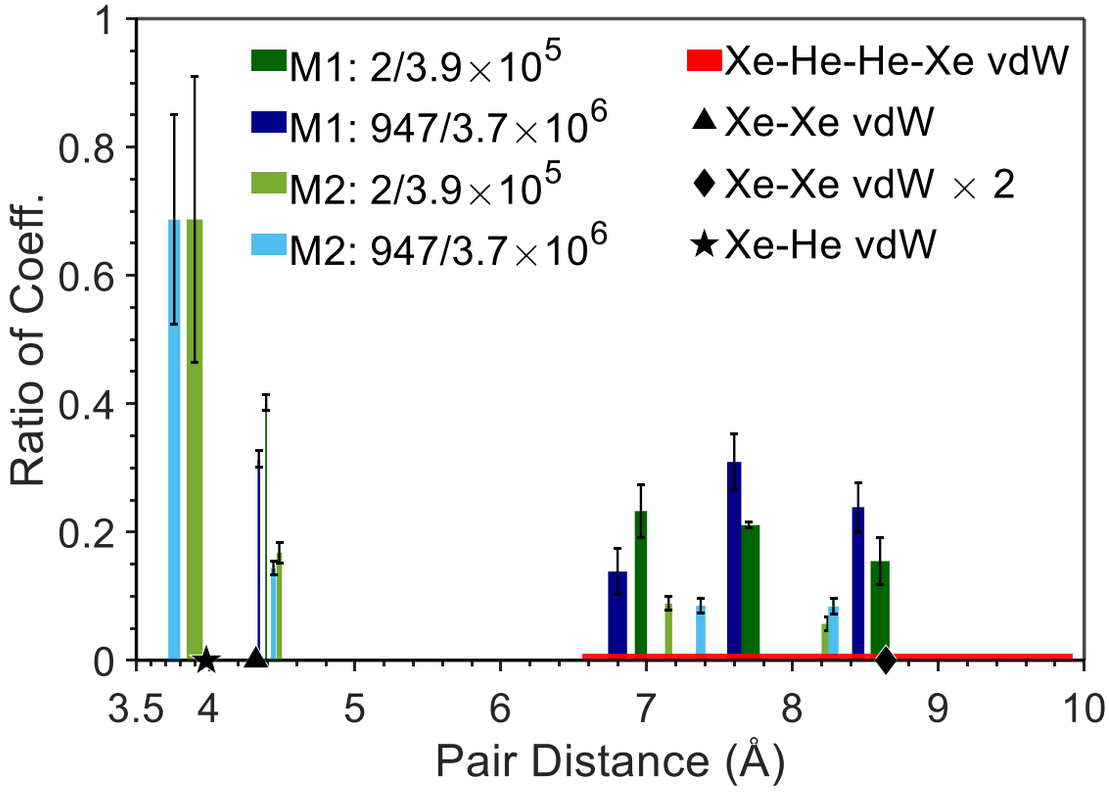

Figure 5. Comparisons of two fitting results for two of the four experimental results: (1) low doping pressure at 18 K, and (2) at 10 K. Model 1 (M1) includes four Xe-Xe pairs, and Model 2 (M2) includes one Xe-He pair and three Xe-Xe pairs. The two numbers in the legend label the numbers of Xe and He atoms in a droplet. The qualities of the fit are slightly better with BIC reductions of 3 for 18 K and 6 for 10 K in model 2.